FEBS Letters 584 (2010) 1091–1096

FEBS Letters

journal homepage: www.FEBSLetters.org

Dimerisation and structural integrity of Heparin Binding Hemagglutinin A from *Mycobacterium tuberculosis*: Implications for bacterial agglutination

Carla Esposito [a], Paola Carullo [b], Emilia Pedone [a], Giuseppe Graziano [c], Pompea Del Vecchio [b], Rita Berisio [a,*]

[a] *Istitute of Biostructures and Bioimaging, C.N.R., I-80134 – Naples, Italy*
[b] *Department of Chemistry "Paolo Corradini", University of Naples Federico II, Complesso Universitario Monte S. Angelo, I-80126, Naples, Italy*
[c] *Department of Biological and Environmental Sciences, University of Sannio, I-82100 Benevento, Italy*

ARTICLE INFO

Article history:
Received 20 January 2010
Revised 12 February 2010
Accepted 16 February 2010
Available online 20 February 2010

Edited by Renee Tsolis

Keywords:
Coiled coil
Tuberculosis
Stability
Agglutination
Dimerisation

ABSTRACT

Heparin Binding Hemagglutinin A (HBHA) is hitherto the sole virulence factor associated with tuberculosis dissemination from the lungs, the site of primary infection, to epithelial cells. We have previously reported the solution structure of HBHA, a dimeric and elongated molecule. Since oligomerisation of HBHA is associated with its ability to induce bacterial agglutination, we investigated this process using experimental and modelling techniques. We here identified a short segment of HBHA whose presence is mandatory for the stability of folded conformation, whose denaturation is a reversible two-state process. Our data suggest that agglutination-driven cell–cell interactions do not occur via association of HBHA monomers, nor via association of HBHA dimers and open the scenario to a possible trans-dimerisation process.

Structured summary:
MINT-7709940, *MINT-7709948*: *HBHA* (uniprotkb:*A5TZK3*) and *HBHA* (uniprotkb:*A5TZK3*) *bind* (*MI:0407*) by *circular dichroism* (*MI:0016*)
MINT-7709966: *HBHA* (uniprotkb:*A5TZK3*) and *HBHA* (uniprotkb:*A5TZK3*) *bind* (*MI:0407*) by *biophysical* (*MI:0013*)
MINT-7709955: *HBHA* (uniprotkb:*A5TZK3*) and *HBHA* (uniprotkb:*A5TZK3*) *bind* (*MI:0407*) by *dynamic light scattering* (*MI:0038*)

1. Introduction

Mycobacterium tuberculosis is an obligate mammalian pathogen that is able to infect many different cells. Although this bacterium has a tropism for the lung, interactions of the organism with respiratory epithelial cells or with the extracellular matrix may also be important in pathogenesis, since these are the first host tissues encountered by mycobacteria when they are transmitted by aerosol. Mycobacterial adherence to epithelial cells is predominantly mediated by the Heparin Binding Hemagglutinin Adhesin (HBHA) [1,2]. This protein binds to heparan sulphate proteoglycans on the surface of epithelial cells and is responsible for extra-pulmonary dissemination of tuberculosis [3]. Binding to target epithelial cells involves the C-terminal lysine-rich domain of the protein, which is exposed at the mycobacterial cell surface [3].

Similar to other adhesins, HBHA is also capable to promote bacterial agglutination [4]. This process, which is typical of lectins, is often associated with post-translational modifications. It is worth noting that native HBHA undergoes post-translational methylation, an event which appears to protect the protein against proteolytic cleavage. However, it has been demonstrated that recombinant non-methylated forms of HBHA are able to promote bacterial agglutination similar to native HBHA [5,6]. The agglutination function of HBHA is a characteristic of its N-terminal part (residues 1–160) [5]. In particular, single-molecule force spectroscopy agglutination has been correlated with the ability of the N-terminal region of HBHA to form multimers [6]. In a previous work, we have determined the solution SAXS structure of both full-length HBHA and a truncated form, deprived of the heparin binding C-terminal domain, $HBHA_{1-160}$ [7]. These results, the sole structural

Abbreviations: HBHA, Heparin Binding Hemagglutinin A; DSC, differential scanning calorimetry; DLS, dynamic light scattering; CD, circular dichroism; PDB, protein data bank; TM, transmembrane helix; $HBHA_{1-160}$, HBHA deprived of its C-terminal arm (residues 161–198); $HBHA_{10-160}$, HBHA deprived of both its C-terminal arm and its N-terminal segment 1–9; $HBHA_{25-160}$, HBHA deprived of both its C-terminal arm and its N-terminal segment 1–24

* Corresponding author. Fax: +390812536642.
E-mail address: rita.berisio@unina.it (R. Berisio).

0014-5793/$36.00
doi:10.1016/j.febslet.2010.02.044

information on HBHA hitherto available, showed that HBHA is characterised by an elongated dimeric structure and provided experimental evidence of the presence of coiled coil regions in $HBHA_{1-160}$ [7]. These data also suggested, consistent with previous findings [5], that bacterial agglutination is to be attributed to interactions between coiled coil motifs of HBHA molecules on the bacterial surfaces [7]. Indeed, coiled coil motifs represent a natural mechanism for guiding and cementing protein–protein interactions. In this scenario, an investigation of HBHA oligomerisation process here reported adds valuable information to the understanding of bacterial agglutination. We have addressed this topic in detail by combining experimental techniques, like differential scanning calorimetry, CD spectroscopy and light scattering with molecular modelling. These studies also provided important information on the structural determinants responsible for HBHA dimerisation and structural integrity.

2. Materials and methods

2.1. 1 Cloning, expression and purification of proteins

$HBHA_{1-160}$ was cloned, expressed and purified as previously reported [7]. The genes codifying for $HBHA_{25-160}$ ($HBHA_{1-160}$ lacking residues 1–24) and for HBH_{10-160} ($HBHA_{1-160}$ lacking residues 1–9) were amplified from *M. tuberculosis* (H37Rv strain) genome by PCR and introduced into the pETM-11 expression vector. Sequenced clones were transformed in the *Escherichia coli* BL21(DE3) strain. Cells were grown to an OD_{600nm} of approximately 0.5 in LB media supplemented with kanamycin (50 μg/ml) at 37 °C and were induced by 1 mM isopropyl-β-D-thiogalactoside (IPTG) for 5 h. The two constructs were purified by a Ni-NTA affinity chromatography (GE Healthcare) equilibrated with 10 mM imidazole, 300 mM NaCl, 50 mM Tris–HCl, pH 8.0 and eluted with a linear gradient of imidazole (10–300 mM). Following histidine tag removal, the protein was further purified by size-exclusion chromatography on Superdex 200 (GE Healthcare).

2.2. Circular dichroism

CD spectra were recorded at room temperature using a Jasco J-810 spectropolarimeter equipped with a Peltier thermostatic cell holder. Molar ellipticity per mean residue, $[\Theta]$ in deg cm^2 $dmol^{-1}$, was calculated from the equation: $[\Theta] = [\Theta]_{obs} \cdot mw/10 \cdot l \cdot C$, where $[\Theta]_{obs}$ is the ellipticity measured in milli-degrees, mw is the mean residue molecular weight, 110.5, 112.3 and 114.8 Da for $HBHA_{1-160}$, $HBHA_{10-160}$, and $HBHA_{25-160}$, respectively, C is the protein concentration in g l^{-1} and l is the optical path length of the cell in cm. Far-UV measurements (260–190 nm) were carried out using a 0.1 cm path length cell and protein concentration 0.3 mg/ml in a 10 mM Tris–HCl, pH 8.0 buffer.

CD spectra were signal averaged over at least three scans and the baseline corrected by subtracting the buffer spectrum. Thermal unfolding curves were recorded in the temperature mode at 222 nm. The concentration dependence of the CD signal was measured in the range 0.1–1.3 mg/ml. Dependence of CD signal on salt concentration was measured at 222 nm using a protein concentration of 0.2 mg/ml and in the presence of NaCl, K_2SO_4 and $MgSO_4$.

2.3. Static and dynamic light scattering

A MiniDAWN Treos spectrometer (Wyatt Instrument Technology Corp.) equipped with a laser operating at 658 nm was used connected on-line to a size-exclusion chromatography or in batch mode (off-line).

Purified $HBHA_{1-160}$ was analysed by size-exclusion chromatography connected to a triple-angle light scattering detector equipped with a QELS module (quasi-elastic light scattering) for mass value and Rh measurements. 500 μl samples (1 mg/ml) were loaded on a S200 10/30 column, equilibrated in 50 mM Tris–HCl, pH 8.0 and 0.15 M NaCl. A constant flow rate of 0.5 ml/min was applied. Elution profiles were detected by a Shodex interferometric refractometer and a mini Dawn TREOS light scattering system. Data were analysed by using Astra 5.3.4.14 software (Wyatt Technology). Determination of molecular masses and hydrodynamic radii are reported as mean values of triplicate experiments. In batch mode, $HBHA_{1-160}$ samples were prepared at 20 °C in 50 mM Tris–HCl, 150 mM NaCl buffer, pH 8.0. A stock solution of $HBHA_{1-160}$, with a concentration of 6 mg/ml, was filtered through a 0.02 μm Millex syringe driven filter unit (Millipore, Bedford, MA). After a further measure of protein concentration, samples were prepared at the following concentrations: 0.2, 1.0, 1.3, 1.7, 2.8 mg/ml. All measurements were registered in triplicates for 2 min acquisition time. The hydrodynamic radius (Rh) of the scattering molecules was derived, using the ASTRA software, from the diffusion coefficient from the Einstein–Stokes equation.

2.4. Differential scanning calorimetry

DSC measurements were carried out on a nano-DSC 6300 (CSC – USA) of high sensitivity and precise baseline repeatability. A scan rate of 1.0 K min^{-1} was chosen for all experiments, and protein concentration ranged from 2.5 to 10 mg/ml. The raw data were converted to an apparent heat capacity by correcting for the instrument calibration curve and the buffer–buffer scanning curve and by dividing each data point by the scan rate and the protein molar concentration in the sample cell. Data analysis was accomplished with in-house programs [8]. The van't Hoff enthalpy change was calculated by the commonly used formula [9]:

$$\Delta_d H(T_d)^{vH} = nRT_d^2 \Delta C_p(T_d)/\Delta_d H(T_d) \quad (1)$$

where T_d is the denaturation temperature corresponding to the maximum of DSC peak, $\Delta C_p(T_d)$ is the height of the excess heat capacity at T_d, $\Delta_d H(T_d)$ is the total denaturation enthalpy change calculated by direct integration of the area of the DSC peak, R is the gas constant and n is 4 or 6 depending on the stoichiometry $N \rightleftarrows D$ or $N_2 \rightleftarrows 2D$. The finding that the calorimetric to van't Hoff enthalpy ratio is close to one is a necessary condition to state that the denaturation is a two-state transition [10].

2.5. Molecular modelling

Modelling of the N-terminal coiled coil was performed using the structure of the basic coiled coil protein from *Eleutherodactylus eligens* (PDB code 3HNW) as a template. The program "O" was used to model point mutations [11]. Energy minimisation of generated 3D-model was done through GROMACS [12] by using Steepest Descent and Conjugate Gradient Algorithms. The coiled coil model was validated using the software SOCKET [13].

3. Results

3.1. Thermal stability of $HBHA_{1-160}$: unfolding is a two-state process

In a previous work, we provided experimental evidence that HBHA and the truncated variant $HBHA_{1-160}$ have a dimeric coiled coil structure [7]. To investigate the unfolding process of HBHA, we studied its thermal stability, by both CD and DSC measurements, over a large protein concentration range and in the presence of various salts. Since the C-terminal domain of HBHA

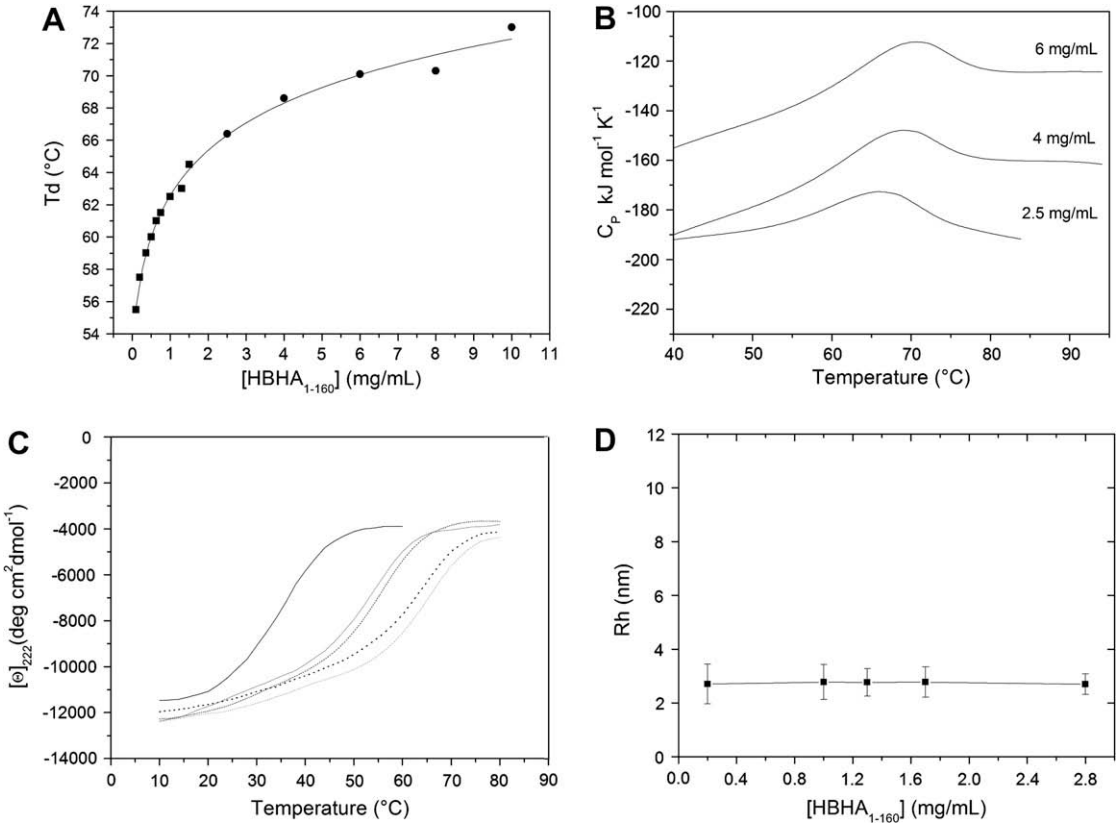

Fig. 1. (A) Unfolding transition temperature T_d of $HBHA_{1-160}$ as a function of protein concentration. Squares and circles are data from CD and DSC, respectively. (B) DSC profiles of $HBHA_{1-160}$ in 50 mM Tris–HCl, 150 mM NaCl, pH 8.0 at increasing protein concentration (mg/ml): (a) 2.5; (b) 4.0, (c) 6.0. (C) Thermal denaturation curves showing dependence of protein stability upon NaCl, $MgSO_4$ and K_2SO_4 concentration. Salt concentrations are: 0.1 M NaCl (grey), 0.3 M NaCl (dashed black), 0.3 M $MgSO_4$ (dotted black) and 0.3 M K_2SO_4 (dashed grey). The reference curve in the absence of salt is shown as a continuous black line. (D) Dependence of $HBHA_{1-160}$ hydrodynamic radius (Rh) on protein concentration, as measured by Dynamic Light Scattering.

is unstructured [7], measurements were carried out on the truncated $HBHA_{1-160}$ variant. Thermal denaturation of $HBHA_{1-160}$ proved to be fully reversible in the selected conditions, pH 8.0, 50 mM Tris–HCl buffer and 150 mM NaCl, according to the reheating criterion. Our results showed that the denaturation temperature of $HBHA_{1-160}$ increased significantly with protein concentration, passing from 55.5 °C at 0.1 mg/ml up to 73.0 °C at 10 mg/ml (Fig. 1A). Thermodynamic analysis of DSC profiles (Fig. 1B) showed that the calorimetric enthalpy change, $\Delta_d H(T_d)$, values agree, within experimental error, with the so-called van't Hoff enthalpy change, $\Delta_d H(T_d)^{vH}$, values calculated in the assumption of a bi-molecular process, of the type $N_2 \rightleftarrows 2D$. For instance, at a protein concentration of 6 mg/ml, $\Delta_d H(T_d) = 360$ kJ/mol and $\Delta_d H(T_d)^{vH} = 380$ kJ/mol. Therefore, CD and DSC measurements consistently show that thermal unfolding of $HBHA_{1-160}$ can be described as a reversible two-state transition of a dimeric species. In this process, monomeric folded $HBHA_{1-160}$ molecules are not present in solution, since dissociation and unfolding of the dimeric structure occur in a concomitant way.

Thermal denaturation experiments were also carried out in the presence of different salt concentrations. As a result, we observed that $HBHA_{1-160}$ is strongly stabilised by an increasing ionic strength. In particular, at a protein concentration of 0.2 mg/ml, T_d varies from 37 °C in the absence of salts to 56 °C in the presence of 0.3 M NaCl (Fig. 1C). A yet more pronounced effect of salt addition on T_d values was observed in the presence of bivalent anions/cations. The addition of 0.3 M sulphate salts (i.e., $MgSO_4$ and K_2SO_4) induces a hyper-stabilisation, as T_d is up-shifted to 64 °C (Fig. 1C).

3.2. Light scattering measurements: $HBHA_{1-160}$ exists solely as a dimer in solution

$HBHA_{1-160}$ was analysed by Static Light Scattering (SLS) and the weight-average molar mass (Mw), was obtained using the ASTRA software. This analysis produced a Mw value of 37 630 Da, which corresponds to a dimeric organisation of the molecule.

To check if the molecular size distribution of HBHA changes at increasing protein concentrations, we also performed Dynamic Light Scattering (DLS). This analysis was carried out at 20 °C using protein concentrations ranging from 0.2 to 2.8 mg/ml. In all conditions, a population of 2.7 ± 0.3 nm hydrodynamic radii (Rh) particles dominated (close to 90% as a mass percent of the sample). As shown in Fig. 1D, no significant variations of Rh values, compatible with the dimeric state of $HBHA_{1-160}$, were observed as a function of concentration (Fig. 1D). These findings show that, in the experimental conditions used, $HBHA_{1-160}$ oligomeric state does not depend on the protein concentration (Fig. 1D) and that no species larger than dimers exist in solution.

3.3. Impact of HBHA N-terminus on structural integrity and modelling N-terminal interactions

Recent analyses of a variety of proteins known to form long two-chain coiled coils have revealed the presence of short regions, often located toward the ends of the heptad sequence region, that foster the initiation of coiled coil formation [14]. In HBHA, heptads are only located at the N-terminal end, since the C-terminus does not possess a coiled coil structure [7]. Consequently, we designed

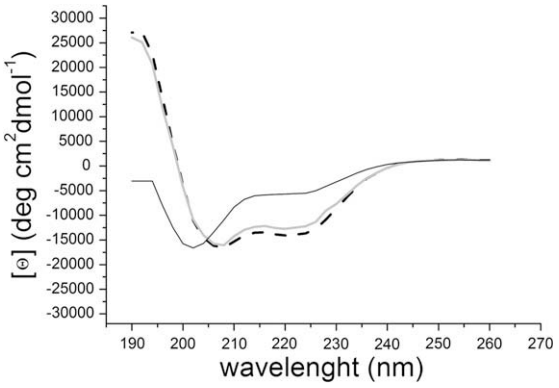

Fig. 2. Superposition of CD spectra of $HBHA_{1-160}$ (dashed black), $HBHA_{25-160}$ (black) and $HBHA_{10-160}$ (grey).

two protein constructs with different deletions of the N-terminal segment, with the aim to observe the impact of these deletions on HBHA dimerisation and structural integrity (Fig. 2). Structure predictions suggest that HBHA helical region starts at residue 14, whereas the coiled coil motif starts at Leu24 (Fig. 3). Therefore, we produced a functional deletion mutant of HBHA lacking the first 24 aminoacids, $HBHA_{25-160}$, and a truncated protein starting at Lys10, $HBHA_{10-160}$, just upstream the beginning of the first α helix. These constructs were cloned, expressed and purified and their stability was measured by CD spectroscopy. Interestingly, far-UV CD spectra recorded at room temperature on $HBHA_{25-160}$ presented a deep minimum at 200 nm and a shoulder at 222 nm (Fig. 2). These characteristics of CD spectra indicate that the $HBHA_{25-160}$ adopts mainly a random coil conformation, with a small amount of α helices (Fig. 2). Differently, $HBHA_{10-160}$ presented a CD spectrum

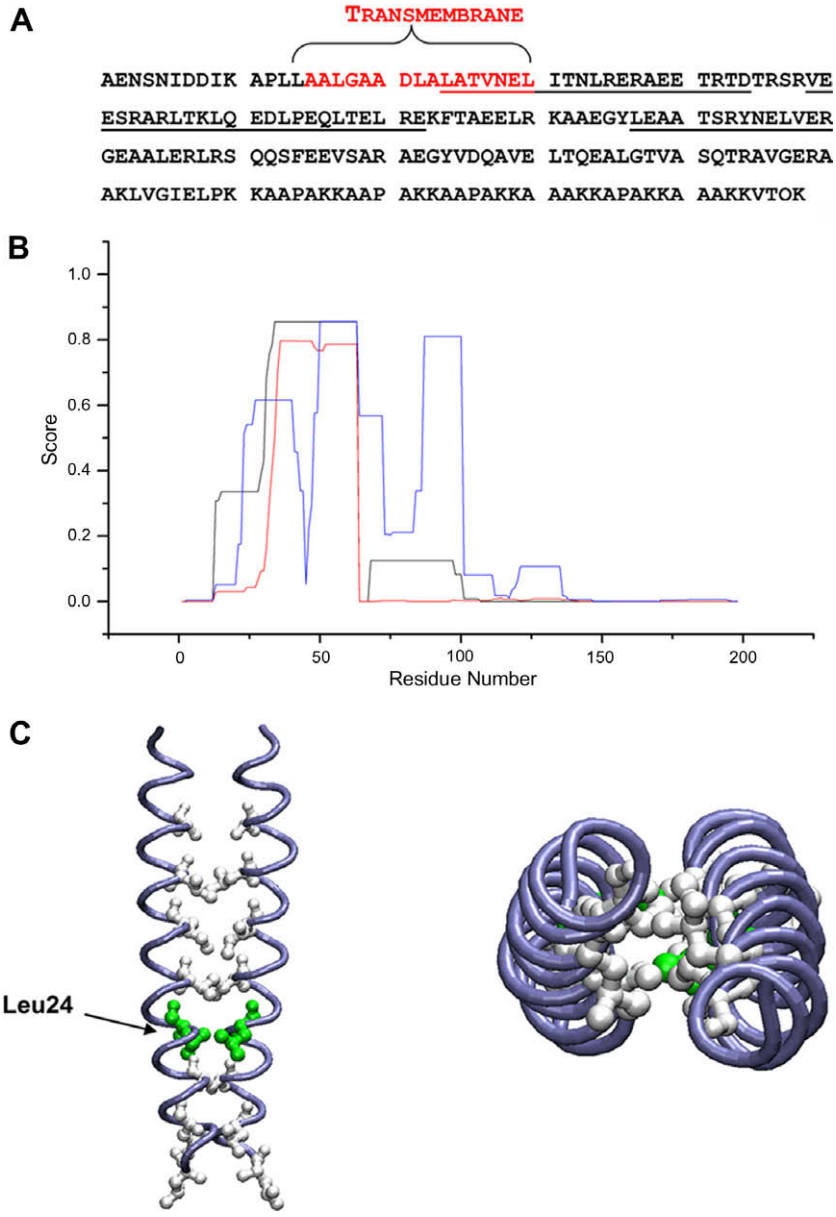

Fig. 3. (A) HBHA sequence with the predicted Transmembrane helix highlighted red. Residues with highest probability of coiled coil formation are underlined. (B) PCOILS (blue) and PAIRCOIL (black) coiled coil prediction scores, calculated using a window of 14 residues and coiled coil dimerisation propensity, calculated using MULTICOIL (green). (C) Side view (left) and top view (right) of the coiled coil model showing packing of hydrophobic residues at 'a' and 'd' positions of the 'abcdefg' heptads. The location of Leu24 is highlighted.

which was completely super-imposable to that of $HBHA_{1-160}$ (Fig. 2).

These results unambiguously showed that the N-terminal region embedded between residues 10 and 24 is of fundamental importance for structural integrity and that hampering N-terminal coiled coil formation strongly affects the stability of HBHA folded conformation.

Based on bioinformatic analyses, a model of N-terminal interactions in HBHA was obtained. As shown in Fig. 3, the highest coiled coil probability characterises three regions embedded between residues 24 and 44, 49 and 72, 87 and 100 (Fig. 3). The first two helices are also predicted, by MULTICOIL [15], to be involved in dimeric coiled coil formation (Fig. 3). A comparative analysis of propensity for Transmembrane (TM) helix formation, carried out using TMpred, MEMSAT and Phobius, consistently shows that only one region of the protein has a tendency to form a TM helix. This region is located at the protein N-terminus and includes residues 16–32, 11–27, 15–30 according to TMpred [16], MEMSAT [17] and Phobius [18], respectively. Therefore, the first helix with high coiled coil propensity (helix 24–44) is both involved in TM helix formation and in dimerisation. This observation has a direct consequence on HBHA dimerisation mode. Namely, the presence of a sole TM region, which is meant to be anchored to the bacterial membrane implies that N-terminal helices forming the dimeric coiled coil must have a parallel arrangement, with each HBHA monomer providing one TM segment of the coiled coil. Based on this observation, molecular modelling of N-terminal helices was carried out using the program "O". The structure of the basic coiled coil protein from *E. eligens* (PDB code 3HNW) was used as a template. The final structure included the N-terminal helical region 14–44, since residues 1–13 are predicted to be unstructured.

This structure was energetically minimised using GROMACS [12]. The resulting model was validated, using the software SOCKET, which analyses the typical structural features of coiled coils, named as knobs-into-holes [13]. Indeed, in typical coiled coils, hydrophobic side chains at 'a' and 'd' positions on one helix act as knobs and dock into holes formed by diamonds of four residues on the partnering helix. This analysis shows that the helix packing of the coiled coil model is particularly tight-knit in the region embedding residues 27–38 (Table 1). Indeed, like in typical parallel helices, 'a' knobs dock into holes formed by '$d^{-1}g^{-1}ad$' residues, whereas 'd' knobs interact with '$adea^{+1}$' holes (superscript numbers refer to either the following (+) or the preceding (−) heptad of the adjacent helix (Table 1). On the other hand, an overrepresentation of alanine residues in 'a', 'b', 'c', 'd', and 'f' positions of the N-terminal segment 14–26 (Fig. 4) results in loose packing of the helices, since alanine residues are not good hole/knob formers. Interestingly, characteristics of the model are in line with the predicted function of the N-terminal residues 13–30 to anchor the mycobacterial cell envelope. Recent cryo-electron microscopy studies have revealed the native three-dimensional organisation of the cell envelope, which is constituted by a peptidoglycan cell wall and an 8 nm thick outer membrane [19,20]. The outer membrane is made of long fatty acids, including mycolic acids, covalently linked to the cell wall peptidoglycans [19,20]. In the model presented in Fig. 4, two hydrophobic residues (like Leu22 and Leu30) and as many as five Ala residues are solvent exposed in each helix of the dimer (Fig. 4). These characteristics well agree with the localisation of the N-terminal residues 13–30 in a hydrophobic environment, such as the mycobacterial outer membrane.

Table 1
Knobs-into-holes interactions in the coiled coil model.

Knobs	Holes
Chain A	
Val27 (d)	Leu24 (a), Val27 (d), Asn28 (e), Ile31 (a)
Ile31 (a)	Val27 (d), Leu30 (g), Ile31 (a), Leu34 (d)
Leu34 (d)	Ile31 (a), Leu34 (d), Arg35 (e), Ala38 (a)
Chain B	
Leu24 (a)	Ala21 (d), Ala23 (g), Leu24 (a), Val27 (d)
Ile31 (a)	Val27 (d), Leu30 (g), Ile31 (a), Leu34 (d)
Leu34 (d)	Ile31 (a), Leu34 (d), Arg35 (e), Ala38 (a)

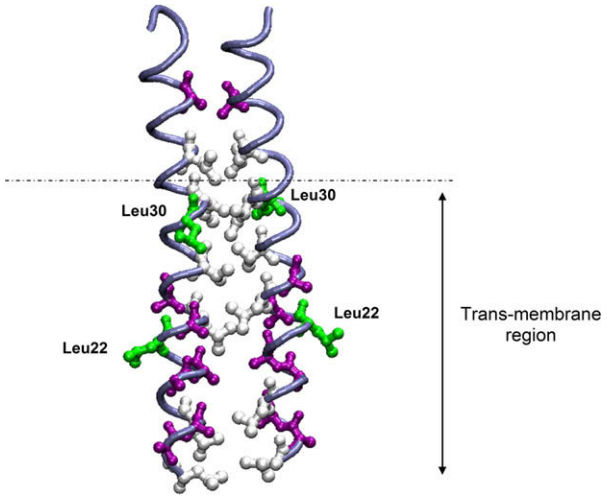

Fig. 4. Side view of HBHA N-terminal coiled coil, showing the high representation of hydrophobic residues in the transmembrane region. Alanine residues are shown in prune, hydrophobic residues other than those in 'a' and 'd' positions are shown in green.

4. Discussion

The coiled coil is probably the most ubiquitous protein–protein interaction motif, as 5–10% of all gene sequences are estimated to encode coiled coil regions [21]. The potential use of coiled coils for biological applications has proven to be immense. Coiled coils are being exploited to function as temperature regulators, antibody stabilizers, anticancer drugs, purification tags, hydrogels, and linker systems [22,23]. In *M. tuberculosis*, the coiled coil domain of the protein HBHA governs agglutination, a process which is important for bacterial pathogenesis [5,7]. By combining experimental and computational techniques, we have investigated the structural basis of HBHA stability and oligomerisation process, a key event in bacterial agglutination [5,7]. For these studies, all HBHA constructs analysed were deprived of the C-terminal arm, as this region does not have a role in agglutination [5,6].

Results reported here consistently confirm the coiled coil nature of HBHA (Fig. 1). DSC experiments have indeed shown that $HBHA_{1-160}$ dimer dissociation and unfolding occur in a single event (two-state transition), as often observed for coiled coils (Fig. 1) [14]. Another characteristics of $HBHA_{1-160}$ that relates its structure to coiled coils is the dependence of its thermal stability on increasing ionic strength (Fig. 1C) [24]. Our results have also evidenced that a small region of $HBHA_{1-160}$, embedded between residues 10 and 24, is determinant for the integrity of the protein folded conformation (Fig. 2). The dependence of protein stability upon presence of a short helical units, which may form a nucleation site during folding, is a typical feature of coiled coil based structures [14,25].

Notably, HBHA is expected to play its biological function in an extracellular environment and exhibits the typical features of soluble proteins, apart from the small transmembrane region which is responsible for HBHA anchoring to the mycobacterial outer membrane. However, our data paradoxically show that the extracellular

portion of $HBHA_{1-160}$ is not sufficient for structural stability in water. Stable dimer formation likely involves the interaction, during the folding pathway, of the two transmembrane N-terminal helical sites which zip-up along the dimer to form the stable coiled coil structure (Fig. 3). This is in line with the parallel arrangement here proposed for the N-terminal two-stranded coiled coil [14] (Fig. 3).

As previously mentioned, bacterial agglutination is to be ascribed to interactions established between coiled coil portions of HBHA [6,7]. We reasoned that a possible aggregation mechanism mediated by HBHA could require that HBHA monomers on bacterial surfaces associate to form coiled coil locked dimers. However, the observed key role of dimerisation for structural integrity, as derived by CD and DSC experiments (Fig. 1A–C), suggested us that agglutination is not due to monomer association. On the other hand, we observed only dimers in solution (Fig. 1D), a finding which makes the possibility of an agglutination process guided by dimer–dimer interactions unlikely. Based on these observations, a mechanism may be surmised which involves bacterial cell–cell interaction via trans-dimerisation of HBHA [26–28]. This process, which involves the formation of trans–cellular dimers, has been observed for various proteins involved in cell adhesion, like the human amyloid precursor protein APP [27,28]. Similar to HBHA, this protein is devoted to the binding of extracellular matrix components, such as heparin [28]. Beside this role, APP is able to promote trans–cellular interactions by forming two types of dimers, denoted as lateral (on the same cell) and adhesive (trans–cellular) [28]. Although a similar mechanism for HBHA needs to be proven, trans-dimerisation may provide an explanation to the ability of HBHA to promote trans–cellular interactions [5], despite its incapacity to either exist as a stable monomer or to form large dimer-based oligomers.

Acknowledgements

This work was funded by MIUR (FIRB-Contract number RBRN07BMCT). P.D.V. is indebted to Maria Rosaria Tiné and Celia Duce for their kind hospitality for the utilization of the nano-DSC at the Department of Chemistry, University of Pisa. We also thank the Centro Interdipartimentale di Metodologie Chimico-fisiche (CIMCF) for technical support.

References

[1] Menozzi, F.D., Bischoff, R., Fort, E., Brennan, M.J. and Locht, C. (1998) Molecular characterization of the mycobacterial heparin-binding hemagglutinin, a mycobacterial adhesin. Proc. Natl. Acad. Sci. USA 95, 12625–12630.
[2] Pethe, K., Alonso, S., Biet, F., Delogu, G., Brennan, M.J., Locht, C. and Menozzi, F.D. (2001) The heparin-binding haemagglutinin of *M. tuberculosis* is required for extrapulmonary dissemination. Nature 412, 190–194.
[3] Pethe, K., Aumercier, M., Fort, E., Gatot, C., Locht, C. and Menozzi, F.D. (2000) Characterization of the heparin-binding site of the mycobacterial heparin-binding hemagglutinin adhesin. J. Biol. Chem. 275, 14273–14280.
[4] Heise, T. and Dersch, P. (2006) Identification of a domain in Yersinia virulence factor YadA that is crucial for extracellular matrix-specific cell adhesion and uptake. Proc. Natl. Acad. Sci. USA 103, 3375–3380.
[5] Delogu, G. and Brennan, M.J. (1999) Functional domains present in the mycobacterial hemagglutinin, HBHA. J. Bacteriol. 181, 7464–7469.
[6] Verbelen, C., Raze, D., Dewitte, F., Locht, C. and Dufrene, Y.F. (2007) Single-molecule force spectroscopy of mycobacterial adhesin–adhesin interactions. J. Bacteriol. 189, 8801–8806.
[7] Esposito, C., Pethoukov, M.V., Svergun, D.I., Ruggiero, A., Pedone, C., Pedone, E. and Berisio, R. (2008) Evidence for an elongated dimeric structure of heparin-binding hemagglutinin from Mycobacterium tuberculosis. J. Bacteriol. 190, 4749–4753.
[8] Barone, G., Del Vecchio, P., Fessas, D., Giancola, C. and Graziano, G. (1992) J. Therm. Anal. 38, 2779.
[9] Privalov, P.L. (1979) Stability of proteins: small globular proteins. Adv. Protein Chem. 33, 167–241.
[10] Zhou, Y., Hall, C.K. and Karplus, M. (1999) The calorimetric criterion for a two-state process revisited. Protein Sci. 8, 1064–1074.
[11] Kleywegt, G.J. and Jones, T.A. (1997) Model building and refinement practice. Methods Enzymol. 277, 208–230.
[12] Van Der Spoel, D., Lindahl, E., Hess, B., Groenhof, G., Mark, A.E. and Berendsen, H.J. (2005) GROMACS: fast, flexible, and free. J. Comput. Chem. 26, 1701–1718.
[13] Walshaw, J. and Woolfson, D.N. (2001) Socket: a program for identifying and analysing coiled-coil motifs within protein structures. J. Mol. Biol. 307, 1427–1450.
[14] Steinmetz, M.O. et al. (2007) Molecular basis of coiled-coil formation. Proc. Natl. Acad. Sci. USA 104, 7062–7067.
[15] Wolf, E., Kim, P.S. and Berger, B. (1997) MultiCoil: a program for predicting two- and three-stranded coiled coils. Protein Sci. 6, 1179–1189.
[16] Hofmann, K. and Stoffel, W. (1993) TMbase – a database of membrane spanning proteins segments. Biol. Chem. Hoppe-Seyler 374, 166.
[17] Jones, D.T., Taylor, W.R. and Thornton, J.M. (1994) A model recognition approach to the prediction of all-helical membrane protein structure and topology. Biochemistry 33, 3038–3049.
[18] Kall, L., Krogh, A. and Sonnhammer, E.L. (2007) Advantages of combined transmembrane topology and signal peptide prediction–the Phobius web server. Nucleic Acids Res. 35, W429–W432.
[19] Hoffmann, C., Leis, A., Niederweis, M., Plitzko, J.M. and Engelhardt, H. (2008) Disclosure of the mycobacterial outer membrane: cryo-electron tomography and vitreous sections reveal the lipid bilayer structure. Proc. Natl. Acad. Sci. USA 105, 3963–3967.
[20] Niederweis, M., Danilchanka, O., Huff, J., Hoffmann, C. and Engelhardt, H. (2010) Mycobacterial outer membranes: in search of proteins. Trends Microbiol., in press.
[21] Newman, J.R., Wolf, E. and Kim, P.S. (2000) A computationally directed screen identifying interacting coiled coils from *Saccharomyces cerevisiae*. Proc. Natl. Acad. Sci. USA 97, 13203–13208.
[22] Hurme, R., Berndt, K.D., Normark, S.J. and Rhen, M. (1997) A proteinaceous gene regulatory thermometer in *Salmonella*. Cell 90, 55–64.
[23] McFarlane, A.A., Orriss, G.L. and Stetefeld, J. (2009) The use of coiled-coil proteins in drug delivery systems. Eur. J. Pharmacol. 625, 101–107.
[24] Meier, M. and Burkhard, P. (2006) Statistical analysis of intrahelical ionic interactions in alpha-helices and coiled coils. J. Struct. Biol. 155, 116–129.
[25] Lee, D.L., Lavigne, P. and Hodges, R.S. (2001) Are trigger sequences essential in the folding of two-stranded alpha-helical coiled-coils? J. Mol. Biol. 306, 539–553.
[26] Tan, K. et al. (2008) Heparin-induced cis- and trans-dimerization modes of the thrombospondin-1 N-terminal domain. J. Biol. Chem. 283, 3932–3941.
[27] Goodger, S.J., Robinson, C.J., Murphy, K.J., Gasiunas, N., Harmer, N.J., Blundell, T.L., Pye, D.A. and Gallagher, J.T. (2008) Evidence that heparin saccharides promote FGF2 mitogenesis through two distinct mechanisms. J. Biol. Chem. 283, 13001–13008.
[28] Soba, P. et al. (2005) Homo- and heterodimerization of APP family members promotes intercellular adhesion. EMBO J. 24, 3624–3634.